Operando observation of the dynamic SEI formation on a carbonaceous electrode by near-ambient pressure XPS

F. Capone, J. Sottmann, V. Meunier, L. Pérez Ramírez, A. Grimaud, A. Iadecola, M. Scardamaglia, J.-P. Rueff, R. Dedryvère

Operando observation of the dynamic SEI formation on a carbonaceous electrode by Near-Ambient Pressure XPS

F. Capone [1,2,3], J. Sottmann [1,2,3,§], V. Meunier [1,4], L. Pérez Ramírez [1,2,3], A. Grimaud [1,4], A. Iadecola [1,3], M. Scardamaglia [5], J.-P. Rueff [2,6], R. Dedryvère [1,7,*]

[1] RS2E, Réseau sur le Stockage Electrochimique de l'Energie, FR CNRS 3459, France

[2] Synchrotron SOLEIL, L'Orme des Merisiers, 91190 Saint-Aubin, France

[3] PHENIX, Sorbonne Université, CNRS, 75005 Paris, France

[4] Chimie du Solide-Energie, UMR 8260, Collège de France, 75231 Paris cedex 05, France

[5] MAX IV Laboratory, Lund University, 225 94 Lund, Sweden

[6] Laboratoire de Chimie Physique-Matière et Rayonnement, Sorbonne Université, CNRS, 75005 Paris, France

[7] IPREM, CNRS, Université de Pau & Pays Adour, E2S-UPPA, 64000 Pau, France

[§] Current address: Hydro Batteries, Hydro Energi AS, Drammensveien 264, NO-0283 Oslo, Norway

* corresponding author : remi.dedryvere@univ-pau.fr

Abstract

The dynamic formation of chemical species composing the solid electrolyte interphase (SEI) layer at the surface of a carbonaceous electrode in a carbonate-based liquid electrolyte was observed in real-time using *operando* Near-Ambient Pressure XPS (NAP-XPS). The potential of the glassy carbon electrode *vs.* metallic lithium was controlled during the XPS experiment. By following the binding energy shifts as a function of the applied potential, we could identify the main SEI species and observe their deposition at the electrode surface during the formation of the SEI. These results demonstrate that NAP-XPS is a powerful tool to investigate the SEI formation and stability in Li- and post-Li-ion batteries, paving the way for future studies on the effect of electrolyte additives and solvent mixtures on battery performances.

1. Introduction

Proper functioning of a Li-ion battery requires the formation of the Solid Electrolyte Interphase (SEI) at the surface of the negative electrode. The role of this layer was described early on for the metallic Li electrode [1], and extended to the case of graphite [2]. The SEI is crucial for normal battery operation because it extends the electrochemical stability window of common electrolytes to the otherwise incompatible very low negative electrode's electrochemical potential. Without the SEI, the electrolyte's constituents (solvents and salt) would be continuously reduced at the negative electrode's surface. The SEI results from the deposition of electrolyte's degradation products at the electrode's surface. It can be thought of as a film that behaves like a solid electrolyte, which means it has a good ionic conductivity permitting proper diffusion/migration of Li^+ ions, and at the same time is electronically insulating, thus preventing further exchange of electrons at the electrode/electrolyte interface and continuous decomposition of the electrolyte. Therefore, the formation of the SEI can be interpreted as a spontaneous self-healing mechanism. In graphite negative electrodes, the SEI also prevents solvent molecules co-intercalation between the graphene sheets during lithium intercalation [3]. Without the SEI formation, this co-intercalation process would lead to irreversible disintegration of the graphite lamellar structure (exfoliation). The presence of the SEI layer, by blocking the co-intercalation process, protects the graphite electrode and enables the reversible intercalation of lithium ions into the graphite structure.

Despite its fundamental role in the battery technology, the SEI suffers from many problems including: stability upon cycling, continuous growth, imperfect electronic insulation, thermal instability. Therefore, the lifetime of the battery is directly linked to the behaviour of the SEI, and thus a full understanding of its formation and aging mechanisms is necessary to improve batteries performances. However, after 40 years of scientific research on this topic, the SEI remains poorly understood, because of its inherent structural and chemical complexity depending on many parameters, such as electrolyte composition, nature of electrode materials, binder, impurities, cycling conditions, temperature, etc... Moreover, it is also difficult to characterize the SEI which is only a few nanometers thick and extremely moisture- and air-sensitive.

To understand the composition, morphology and associated formation mechanisms of the thin SEI surface film, surface-sensitive spectroscopies like infrared spectroscopy (FTIR) [4,5], X-ray Photoelectron Spectroscopy (XPS) [6], Auger Electron Spectroscopy (AES) [7], Secondary Ion Mass Spectrometry (ToF-SIMS) [8] or microscopies like Atomic Force

Microscopy (AFM) [9] or Scanning Tunneling Microscopy (STM) [10] have been used. Electrochemical Quartz Crystal Microbalance (EQCM) [11], Differential Electrochemical Mass Spectrometry (DEMS) [12], or thermo-analytical techniques like Temperature Programmed Desorption (TPD) [13] and Differential Scanning Calorimetry (DSC) [14] have been also employed to study SEI formation and degradation. Moreover, bulk analysis techniques like NMR [15,16] have also been used to characterise the SEI, thanks to the possibility to distinguish the signal from the bulk electrode to the that of the SEI.

Among all these techniques, XPS occupies a prominent place due to its probing depth of a few nanometers and its sensitivity to the chemical composition, oxidation states and chemical environments of probed elements. However, this surface sensitivity requires removing the electrolyte from the electrode's surface by rinsing it with pure solvent to avoid salt precipitation at the surface, prior to drying the electrode and transferring it to vacuum. This *ex situ* preparation method is widely used in the battery community. It is well mastered via the use of oxygen- and water-level controlled argon atmosphere gloveboxes directly connected to XPS spectrometers, or through vacuum transfer chambers, and has led to most of the main scientific insights on the SEI, which are still relevant today. However, such experimental conditions are obviously quite far from the actual conditions existing in a battery during its operation, where the electrodes are constantly in contact with the electrolyte. Although the name SEI (Solid Electrolyte Interphase) suggests it is a solid film, its structure is quite complex. The inner parts are supposed to be rather insoluble in the electrolyte; however, this is much more questionable for the outer parts, especially when the ionic force is modified by dilution when the electrode is rinsed in pure solvent. Moreover, there is a significant delay (from several hours to several days) between the end of the electrochemical charge or discharge of the battery and the XPS experiment, which prevents us from the observation of dynamic effects (formation of metastable components in the SEI, for example) because the *ex situ* sample is in a relaxed state. This is the reason why the battery community is nowadays focusing on the development of *operando* approaches.

The development of Near-Ambient Pressure XPS (NAP-XPS) in the last 15 years has offered new opportunities for the study of solid/gas and solid/liquid interfaces [17,18], with possible applications for the *in situ* or *operando* study of the SEI. This methodology based on a pressure gradient between the analysis chamber containing the sample (P ~ 1-100 mbar) and the photoelectron analyzer (P ~ 10^{-9} mbar) thanks to successively differentially pumped sections, was early proposed by H. Siegbahn. [19] It allows the analysis of liquids by XPS in a rough vacuum, depending on their vapour pressure. Due to important technical difficulties,

NAP-XPS has become widely available only recently, especially thanks to synchrotron radiation sources, and is now even proposed in commercial XPS machines with possible extension to high-kinetic energy operations (NAP-HAXPES). It has become an important tool for *in situ*/*operando* investigation of solid-gas interfaces in the field of heterogeneous catalysis. [20] In the field of electrochemistry, Axnanda *et al.* [21] proposed in 2015 an *operando* approach consisting of a dip & pull method to study the solid-liquid interface between a platinum electrode and an aqueous electrolyte by maintaining the applied potential between the Pt working electrode and a Ag/AgCl reference electrode during XPS measurement. Application to Li-ion batteries came several years later when two teams reported the NAP-XPS study of carbonate-based organic liquid electrolytes in contact with metallic Li [22] or with a positive electrode material (V_2O_5) [23], although without applying any potential. I. Källquist *et al.* [24] extended the *operando* dip & pull method to Li-ion batteries in 2021 by the NAP-XPS study of Au and Cu model electrodes in contact with the electrolyte (1M $LiClO_4$ in propylene carbonate, PC) and a metallic Li ribbon as reference electrode, as a function of applied potential. This method was also used for a $Li_4Ti_5O_{12}$ (LTO) negative electrode [25]. By looking at the photoelectron kinetic energy shift (and thus, apparent binding energy shift) of the electrolyte species as a function of the applied potential on the electrode, measured at the surface of the electrolyte meniscus, these pioneering studies demonstrated that *operando* NAP-XPS can provide useful information about the charge transfer of Li^+ ions occurring at the electrode/electrolyte interface. However, the direct XPS chemical analysis of the SEI was not possible in these studies due to the great thickness of the electrolyte liquid film covering the electrode's surface, which exceeds the probing depth of XPS.

In the present work, to overcome this problem, we propose to focus the XPS analysis on the thin precursor film preceding the wetting front of the electrolyte meniscus. The thickness of this precursor film, which is roughly between the single molecular layer and 10 nm [26,27,28], makes the direct XPS analysis of the SEI possible. However, in order to pinpoint the exact location of the precursor film (whose size is about 50-100 µm) during the measurement, it is necessary to simultaneously detect the C 1s signals of the working electrode, electrolyte and SEI to precisely adjust the position of the sample. To this aim, it is necessary to use a carbonaceous electrode. But a common porous graphite electrode, as used in commercial Li-ion batteries, is not suitable for this kind of *operando* study of the SEI because its rough surface does not allow the formation of a constant thickness liquid film. Alternatively, a polished glassy carbon (GC) electrode is not porous, has a flat surface, a good electronic conductivity, and since it is a carbonaceous material, it is much closer to the real case of graphite than model metallic

electrodes. Indeed, since there is no need for Li^+ intercalation to form the SEI, whose formation is driven by the potential of the electrode, it was shown that the composition of the SEI formed at a GC electrode's surface is similar to that formed onto graphite [29,30,31]. Therefore, we propose in this study to perform the *operando* NAP-XPS investigation of the SEI formation at the surface of a GC electrode.

2. Experimental section

2.1. Electrochemical cycling

Electrochemical experiments were carried out according to the dip & pull method developed by Axnanda *et al.* [21] and Källquist *et al.* [24] using the electrochemical cell environment available at the HIPPIE beamline in MAX IV synchrotron (Lund, Sweden) [32]. Electrodes were immersed in an electrolyte composed of 1 $mol.L^{-1}$ of $LiPF_6$ dissolved in propylene carbonate (PC) in a polyether ether ketone (PEEK) beaker in the NAP-XPS analysis chamber. The choice of PC was dictated by the need for a solvent having a low vapour pressure. When a more common formulation was tried (LP57, *i.e.* 1M $LiPF_6$ in EC:EMC in a 3:7 ratio), the high vapour pressure of EMC resulted in a saturation of the analysis chamber with gaseous EMC at a too high pressure to obtain a good XPS signal from the sample. Glassy carbon (GC) (SIGRADUR, HTW) was used as working electrode and a metallic Li ribbon (Sigma Aldrich, 99.9%, thickness 0.38 mm) was used as reference and counter electrode. The GC electrode was first polished with a rotating disk polishing machine and polishing solutions with grains up to 4µm in diameter. It was then rinsed and sonicated before being dried and transferred to an argon filled glovebox (H_2O and O_2 < 0.1 ppm). There, it was sealed in a glass container and then in an aluminium bag. The Li ribbon was stored in the glovebox and packed in the same way. Before every NAP-XPS experiment, the surface of the Li ribbon was mechanically scraped to obtain a fresh and non-oxidized surface. A custom-designed glovebox attached to the analysis chamber is available at HIPPIE and is equipped with a moisture detector (Mbraun, MB-MO-SE1) and an oxygen detector (Mbraun, MB-OX-SE1). It was constantly filled and cycled with high-purity argon gas, thus ensuring an inert atmosphere over the whole experiment.

The electrochemical procedure carried out for the dip&pull experiments was performed using a Biologic SP150 potentiostat and the EC-Lab software. To obtain the desired procedure, a combination of Constant Voltage Holding (CstV) and Linear Sweep Voltammetry (LSV) was adopted. From Open Circuit Voltage (OCV) (around 3V *vs.* Li^+/Li for our system), an LSV would sweep the voltage as in common cyclic voltammetry to the first desired step, with a rate

of 2mV/s. There, the voltage is kept constant until the current passing in the system stabilizes. After that, the electrode is pulled out of about 3 mm to create the electrolyte meniscus, and the XPS measurement was performed. Then the electrode is dipped back to the starting position and the procedure moves to the next LSV to continue to the next voltage step.

2.2. NAP-XPS experiments

HIPPIE is a soft X-ray beamline with an accessible photon energy range from 250 to 2200 eV equipped with a ScientaOmicron HiPP-3 electron energy analyzer. The photon energy was fixed at 1800 eV, which corresponds to a good compromise between the probing depth and the photoelectron throughput. The beam impinges on the sample surface with an incident angle of 35° and the spot size at the sample position is 100×25 μm^2 (H×V). The photoelectrons were collected at normal emission. No charge neutralizer was used. The spectra are presented without any binding energy (B.E.) calibration to directly observe the B.E. shift provoked by the applied potential between the two electrodes.

The XPS analysis chamber is vented with argon for the sample mounting, then the pressure is gradually decreased to ensure gentle bubbling of dissolved gases in the electrolyte, until reaching a pressure of ~ 0.25 mbar (close to the vapour pressure of PC) and maintained constant during the whole experiment.

3. Results and discussion

The principle of our dip & pull NAP-XPS experiment is illustrated in Figure 1. Additional pictures and photos are available in the supplementary information (Fig. S1). In this approach, we focus on the electrolyte precursor film formed on the glassy carbon (GC) electrode. This precursor film is formed when the surface of a solid is wetted by a liquid in the presence of a third gaseous phase (PC vapour in our case). The macroscopic wetting front is then preceded by the very thin (~ 1 nm) precursor film. [28] In our case, the precursor film thickness is compatible with the probing depth of XPS at a photon energy of 1800 eV. The exact location of the precursor film was obtained by real-time observation of the same C 1s spectrum of the GC electrode, the electrolyte (PC) and additional species from the SEI, by tuning the height of the electrode with respect to the electrolyte solution surface in the beaker. This was possible thanks to the carbonaceous nature of the GC electrode. The vertical size of the precursor film

has been experimentally estimated to be around 100 µm by scanning the GC electrode. We were also able to prove the film stability in the timescale of the experiment, which is explained by the fact that the XPS analysis chamber was saturated by PC vapour.

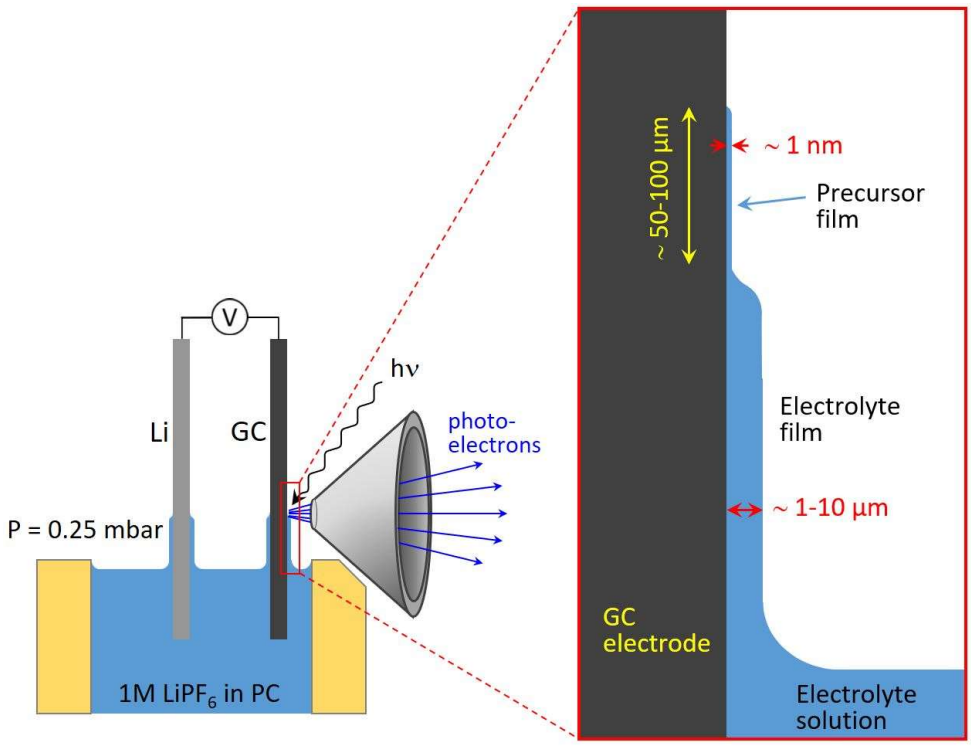

Figure 1 : Schematic view of the dip & pull experiment. The glassy carbon and Li electrodes are partially immersed in the electrolyte during NAP-XPS measurements. The vertical position of the electrodes is adjusted to focus the analysis on the precursor film.

3.1. Electrochemical results

At first, we have tested the good operation of the GC||Li cell in our in-house glovebox filled with controlled argon atmosphere (P = 1 atm), before using this cell in NAP conditions at the synchrotron beamline. This electrochemical assessment is available as supplementary information (Figure S2).

The electrochemical curves recorded with the *operando* setup at the synchrotron beamline during the NAP-XPS experiment are presented in Figure 2. The experiment was performed according to the procedure reported in previous studies [24,25]. In these conditions, the cell was exposed to a 0.25 mbar pressure of PC vapour. Figure 2a displays the applied voltage *vs.* time

profile from Open Circuit Voltage (OCV) to 0.05V *vs.* Li^+/Li. The dip & pull experiment is carried out at each potential step: the electrode is dipped rapidly into the electrolyte, then the potential is decreased at 2 mV/s rate until the next potential step is reached. After relaxation of the current intensity, the electrode is pulled out of the electrolyte solution (at constant voltage) for the NAP-XPS experiment. The obtained current intensity *vs.* voltage curve shown in Figure 2a is similar to that obtained in-house (Figure S2) although the experimental conditions are different, which validates our electrochemical setup in these NAP-XPS conditions. Figure 2b shows the resulting current intensity *vs.* time curve. A small jump in the current intensity appears once the electrodes are pulled out before the end of each potential step, because the surface of electrodes in contact with the electrolyte decreases and therefore less current can flow (see for example the jumps at t = 0.7h, 1.8h, 3.0h, 4.1h, 4.9h, 5.7h, etc. in Figure 2a).

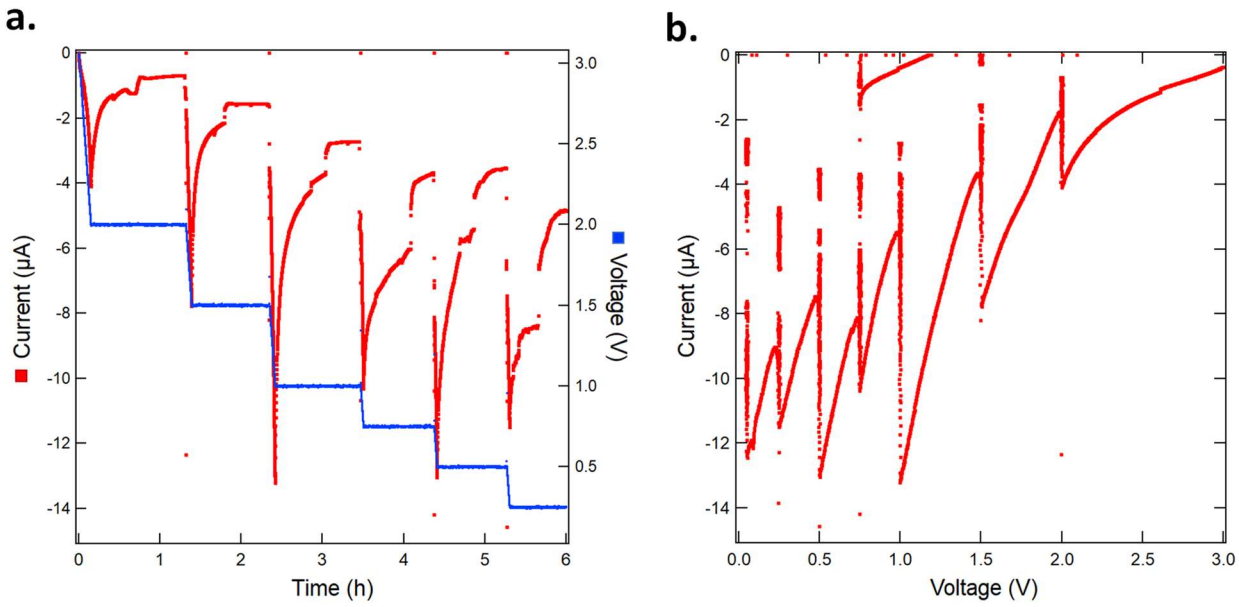

Figure 2 : Electrochemical behaviour of the cell in the NAP-XPS analysis chamber during the dip & pull experiment: **(a)** Applied voltage (blue) and current intensity (red) *vs.* time curves, showing current jumps due to electrode withdrawal in the middle of each potential step (periods corresponding to the XPS experiments). **(b)** Current intensity *vs.* voltage curve.

3.2. NAP-XPS results

Two different electrode locations were probed: *(i)* the surface of the electrolyte film covering the GC electrode, *(ii)* the surface of the thin electrolyte's wetting precursor film (Figure 1).

Although the electrolyte film is too thick to allow detection of the GC electrode's signal, it gives valuable information about the electrolyte itself and the charge transfer process at the GC electrode/electrolyte interface. Figure 3a shows the typical shape of the obtained C 1s spectra, here as an example the spectrum recorded at the end of the electrochemical experiment (0.05 V vs. Li^+/Li^0). Despite the significant shift towards higher B.E. due to the applied potential, the main peaks can be attributed to the three different carbon environments in the PC solvent. The two peaks at 290.6 and 294.3 eV, with an intensity ratio of 2/1, are attributed to C-O and CO_3 carbon environments, respectively. The third peak at ~288.5 eV corresponds to the CH_3 group. Its intensity is expected to be the same as the CO_3 component due to the structure of the PC molecule, however here it is enhanced by the presence of an extra hydrocarbon (CH_x) surface contamination, as it is commonly observed in XPS analysis and explained by the presence of hydrocarbon species in the analysis chamber.

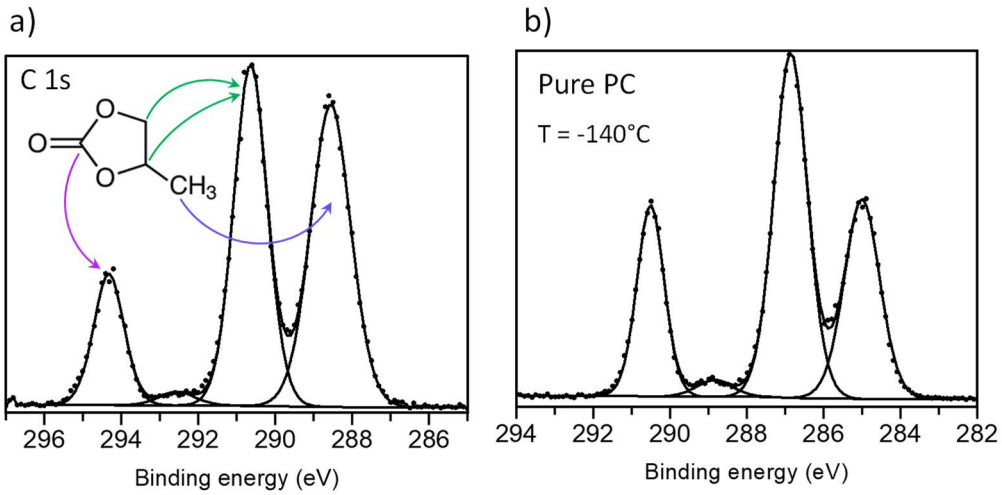

Figure 3 : **(a)** NAP-XPS C 1s spectrum recorded at room temperature at the surface of the electrolyte film covering the GC electrode (applied potential: 0.05 V vs. Li^+/Li); **(b)** C 1s spectrum of pure PC solvent, as a frozen liquid drop at T = -140°C under ultra-high vacuum (in-house XPS spectrometer at hν = 1486.6 eV).

It is worth noting that an additional weak peak was observed at ~292.5 eV, which could be assigned to the presence of carbon bound to two oxygen atoms. Since this carbon environment is absent in the PC molecule, it was first important to make sure that this weak peak cannot be attributed to chemical species ensuing from the electrochemical reaction. To this aim, we recorded the XPS spectrum of pure PC solvent as a frozen liquid drop at T = -140°C under ultra-high vacuum using in-house XPS for comparison. The obtained C 1s spectrum is shown in Figure 3b. In this case, no potential was applied and thus there is no B.E. shift with respect to expected values. No extra hydrocarbon (CH_x) surface contamination was observed at low temperature since CO_3 and CH_3 components display the same intensity. Besides these differences, the two spectra are very similar and the weak peak (at ~ 289 eV in Figure 3b) was observed in both cases. We conclude that such peak may originate from the presence of an impurity in the PC solvent, or possibly of a weak amount of a degradation product resulting from exposure to the X-ray beam (however, the low brilliance of the in-house XPS photon source compared to the synchrotron conditions prevents comfortably from beam degradation).

We now turn to the results of the NAP-XPS dip & pull experiments. Figure 4a displays the evolution of C 1s spectra recorded on the thick liquid film covering the electrode, as a function of the applied potential. A linear energy shift of C 1s spectrum can be observed as a function of applied voltage and two regions can be distinguished, as displayed in Figure 4b: *(i)* between 2.84 V (OCV) and 1 V *vs.* Li^+/Li, and *(ii)* between 1 V and 0.05 V *vs.* Li^+/Li. This behaviour has been already observed in previous works [24,25] and it can be explained by considering the influence of the applied potential on the emitted photoelectrons. In our case, the surface of the GC electrode is negatively charged; when the applied potential with respect to the Li reference electrode decreases, an influx of electrons comes to the GC electrode through the external circuit, facilitating the ejection of the photoelectrons. This means that the kinetic energy of the photoelectrons coming from the GC electrode is increased, and thus their apparent B.E. is decreased, compared to electrolyte's species. However, since the GC electrode is grounded to the spectrometer, the apparent B.E. of the photoelectrons emitted from the electrode is actually unchanged, while the apparent B.E. of electrolyte species, which are not grounded to the spectrometer, are shifted in the opposite way (towards higher energies).

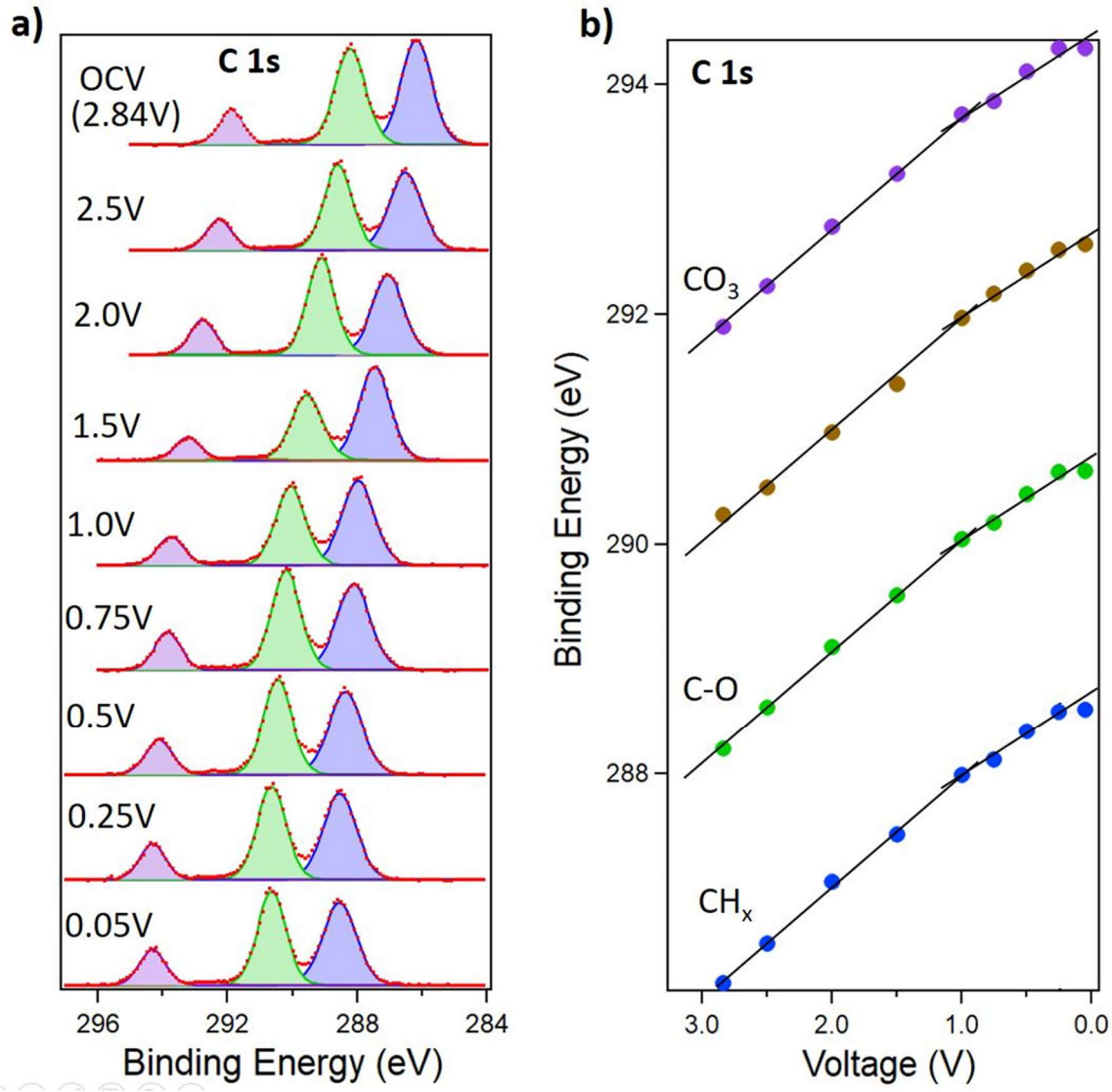

Figure 4 : **(a)** NAP-XPS C 1s spectra recorded at the surface of the thick electrolyte film as a function of the applied potential *vs.* Li^+/Li; **(b)** Evolution of the binding energies (B.E.) of the four identified C 1s components (without any B.E. calibration).

In Figure 4a, the C 1s signal of the GC electrode is not observed, meaning the thickness of the electrolyte film is higher than the XPS probing depth. Since there is a direct link between the applied potential and the created electric field in the vicinity of the electrode's surface, we expect a linear dependency of 1 eV/V of the B.E. shift of electrolyte species. This is actually observed in the first region of Figure 4b, *i.e.* between 2.84 V (OCV) and 1 V *vs.* Li^+/Li. In the second region corresponding to lower voltages between 1 V and 0.05 V *vs.* Li^+/Li, we clearly observe a weaker slope estimated at ~ 0.7 eV/V. This deviation from the expected slope was

explained by Källquist *et al.* as originating from the charge transfer occurring at the electrode/electrolyte interface, leading to a change in the electrostatic potential of the electrolyte [24]. Furthermore, the change of slope in B.E. at 1 V *vs.* Li^+/Li corresponds to the highest reduction peak observed during the Linear Sweep Voltammetry experiment. This additional evidence supports the idea that the change is a result of the SEI formation.

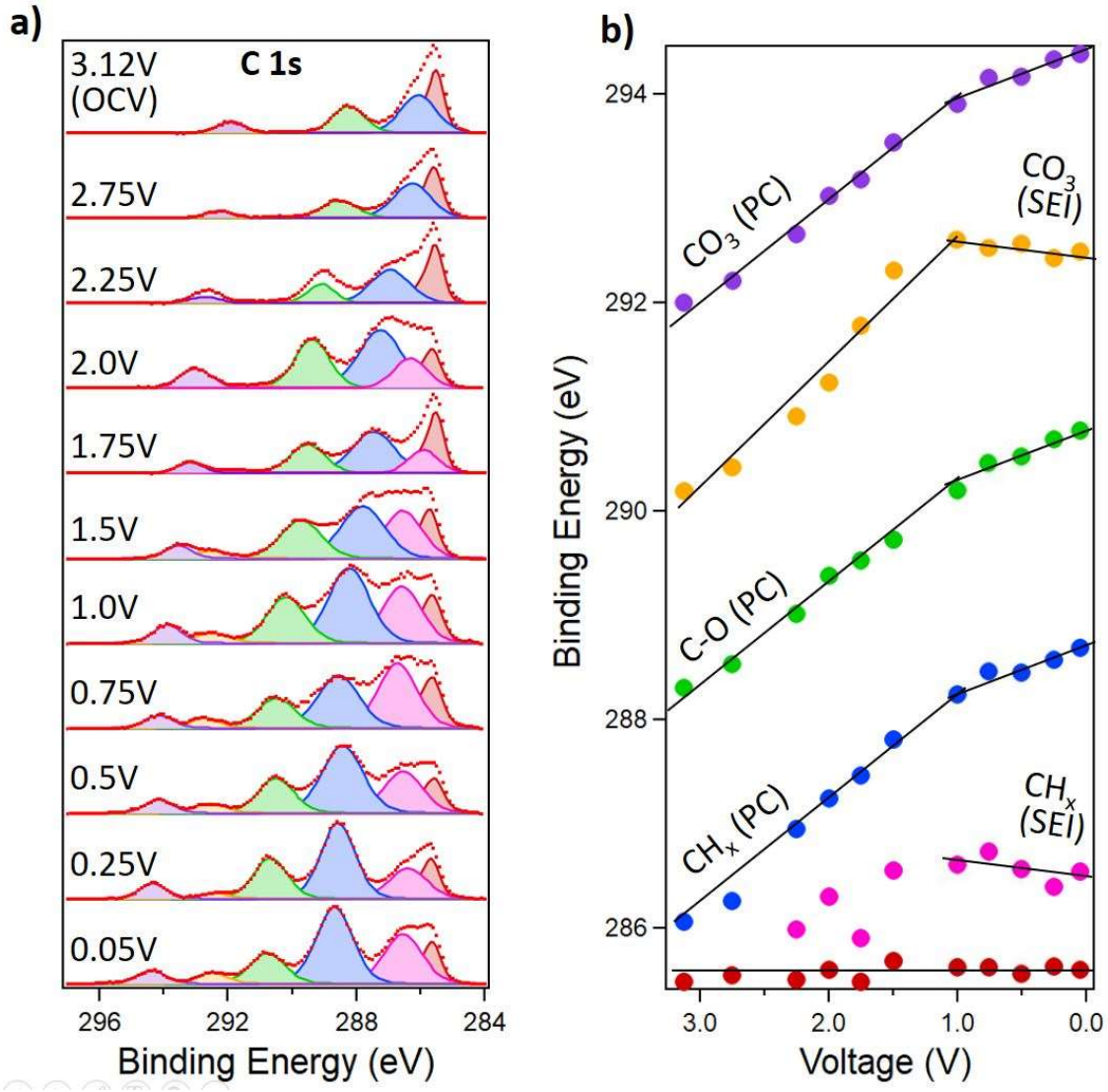

Figure 5 : **(a)** C 1s NAP-XPS spectra recorded on the thin electrolyte's precursor film as a function of the applied potential *vs.* Li^+/Li; **(b)** Evolution of the B.E. of all identified C 1s components (without any B.E. calibration).

If we focus now on the region of the GC electrode corresponding to the thin electrolyte precursor film, the results are significantly different, as detailed in Figure 5. Although the three main C 1s components of PC solvent are still observed, we can detect additional peaks. The first difference, as shown in Figure 5a, is the presence of the GC electrode's C 1s signal at B.E. ~285.5 eV, because the thickness of the precursor film is lower than the XPS probing depth at 1800 eV photon energy. Since the GC electrode is grounded to the spectrometer, its B.E. does not depend on the applied potential, as explained above. Only a fluctuation of ± 0.1 eV is observed, which corresponds to the error of the measurement. The spectrum of the GC electrode has an asymmetric shape, as usually observed for carbonaceous electronic conductors (graphite, carbon black, etc.).

Besides the peaks of GC electrode and PC solvent, two additional C 1s components are observed. The first one (yellow/orange in Figure 5) is observed between the two components corresponding to C-O and CO_3 environments of PC (292.5 eV at 0.05V). Its intensity increases when the applied voltage decreases, and reaches up to 80% of the intensity of the CO_3 component of PC. Therefore, this component has a different origin compared to the weak parasitic component discussed in Figure 3 (at least, below 2V). Not only its intensity is much greater (the original parasitic peak is hidden by this one), but also its behaviour regarding the applied potential is completely different. Indeed, we can see in Figure 5b that after a positive linear B.E. shift between OCV and 1 V *vs.* Li^+/Li, it undergoes a negative shift between 1 V and 0.05 V. The observed positive linear shift in the first region is ~1.1 eV/V, then the negative shift is about -0.15 eV/V. Therefore, we propose hereafter an explanation for this peculiar behaviour with respect to the applied potential.

Figure 6 displays a schematic view of the potential profile from the surface of the GC electrode to the bulk electrolyte when a negative voltage is applied. In the absence of any SEI formation, the applied potential leads to the formation of the Electric Double Layer (EDL) at the vicinity of the electrode's surface, as described by the Gouy-Chapman-Stern model [33], which is composed of the compact (Stern) layer and the diffuse layer. The potential drop is caused by the concentration gradient of ions with opposite charge as a function of the distance from the surface to the electrolyte. When an SEI is formed at the surface of the GC electrode, the potential drop will take place within the SEI due to its electronic insulating character [34,35], as schematized in Figure 6. Because of the complexity of the SEI structure, it is impossible to identify the SEI limit like for the inner and the outer Helmholtz planes (IHP and OHP) of the

EDL, and to date there is no definition of the limit between the outer part of the SEI and the electrolyte.

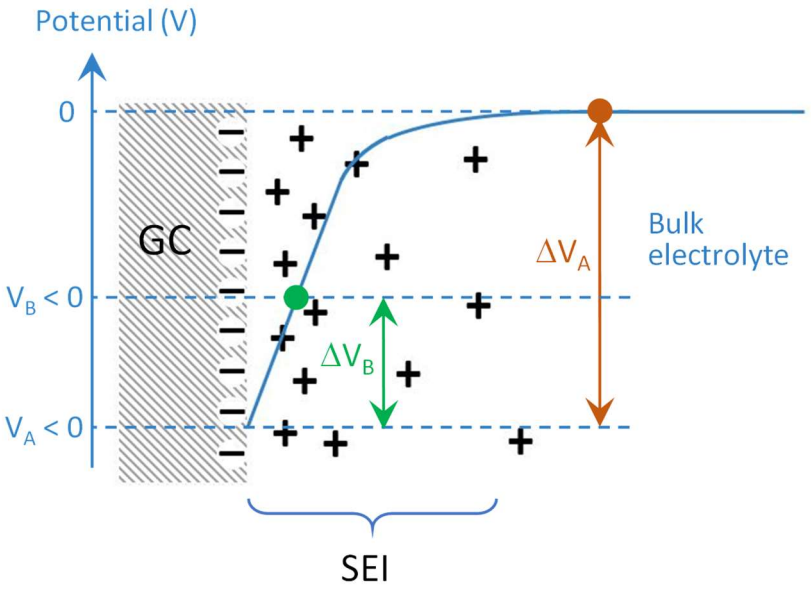

Figure 6 : Schematic view of the potential drop from the surface of the negatively charged GC electrode to the bulk electrolyte. The + symbol stands for the excess of positive charges. Negative charges in the electrolyte and the SEI are not represented.

The B.E. shift of electrolyte species (blue, green and violet components in Figure 5) with respect to the GC electrode is therefore due to the potential difference between the electrode surface and the bulk electrolyte (ΔV_A in Figure 6). In the first region of Figure 5b (between 3.1 V and 1 V *vs.* Li^+/Li), the 1 eV/V linear slope of the B.E. of the yellow/orange C 1s component is in agreement with its assignment to a chemical species of the electrolyte. However, the negative shift of -0.15 eV/V observed below 1 V *vs.* Li^+/Li implies that the potential difference between this species and the GC electrode surface decreases (ΔV_B in Figure 6). This indicates that the associated chemical compound is no more located in the bulk of the electrolyte but closer to the GC electrode, where the potential difference varies with the distance from the electrode's surface, and that it gets closer to the GC electrode surface when the applied voltage decreases. This corresponds to the deposition of species in the SEI when the potential decreases. Given the B.E. difference between this C 1s component and the GC electrode, we can conclude that this component corresponds to an inorganic carbonate (carbon

in CO_3 environment, either Li_2CO_3 or a lithium alkylcarbonate $ROCO_2Li$ formed by reductive decomposition of PC at the surface of the electrode, like $LiO_2CO\text{-}CH(CH_3)CH_2\text{-}OCO_2Li$ (lithium propylene dicarbonate) for example). The chemical nature of these inorganic carbonates probably changes when the potential decreases during the experiment because the reductive decomposition reactions are driven by the potential. For the first time, these results represent the real-time direct observation of the deposition of chemical species at the surface of the electrode to build the SEI when the applied potential decreases using NAP-XPS.

Further information can be retrieved from the analysis of the other additional C 1s component (pink in Figure 5a) which is observed between the GC electrode component and the CH_x component of PC (286.7 eV at potential 0.05V). There is a significant error in the position of this peak at high applied potentials because it is strongly overlapped with the CH_x component of PC. However, at lower potentials the measurement of its B.E. is more accurate, and it is interesting to notice that this peak undergoes almost the same negative B.E. evolution as the yellow/orange additional component (*i.e.* -0.15 eV/V), which means it could be attributed to the same chemical species. For example, it could be assigned to the CH_3 group of lithium propylene dicarbonate, but it could also originate from other chemical species of the SEI containing hydrocarbon groups (CH_x).

Additional proofs about the formation of the SEI were provided by the analysis of O 1s and F 1s XPS core peaks. Figure 7 displays O 1s spectra and the evolution of their B.E. as a function of the applied potential. At the beginning of the electrochemical experiment (OCV and potentials above 2V) the O 1s spectra are composed of two peaks attributed to C=O and C-O oxygen environments in the PC molecule. More details about this attribution are given in Figure S3 (supplementary information). The evolution of their B.E. as a function of applied potential follows the same trend as the C 1s components assigned to PC, *i.e.* + 1 eV/V for potentials greater than 1V and ~ +0.5 eV/V for potentials lower than 1V *vs.* Li^+/Li. The third O 1s component, on the other hand, follows the same evolution as the C 1s component attributed to inorganic carbonates of the SEI, more precisely its B.E. shift follows a +1.1 eV/V slope for applied potentials higher than 1V, and undergoes the same negative shift of -0.15 eV/V for potentials lower than 1V *vs.* Li^+/Li.

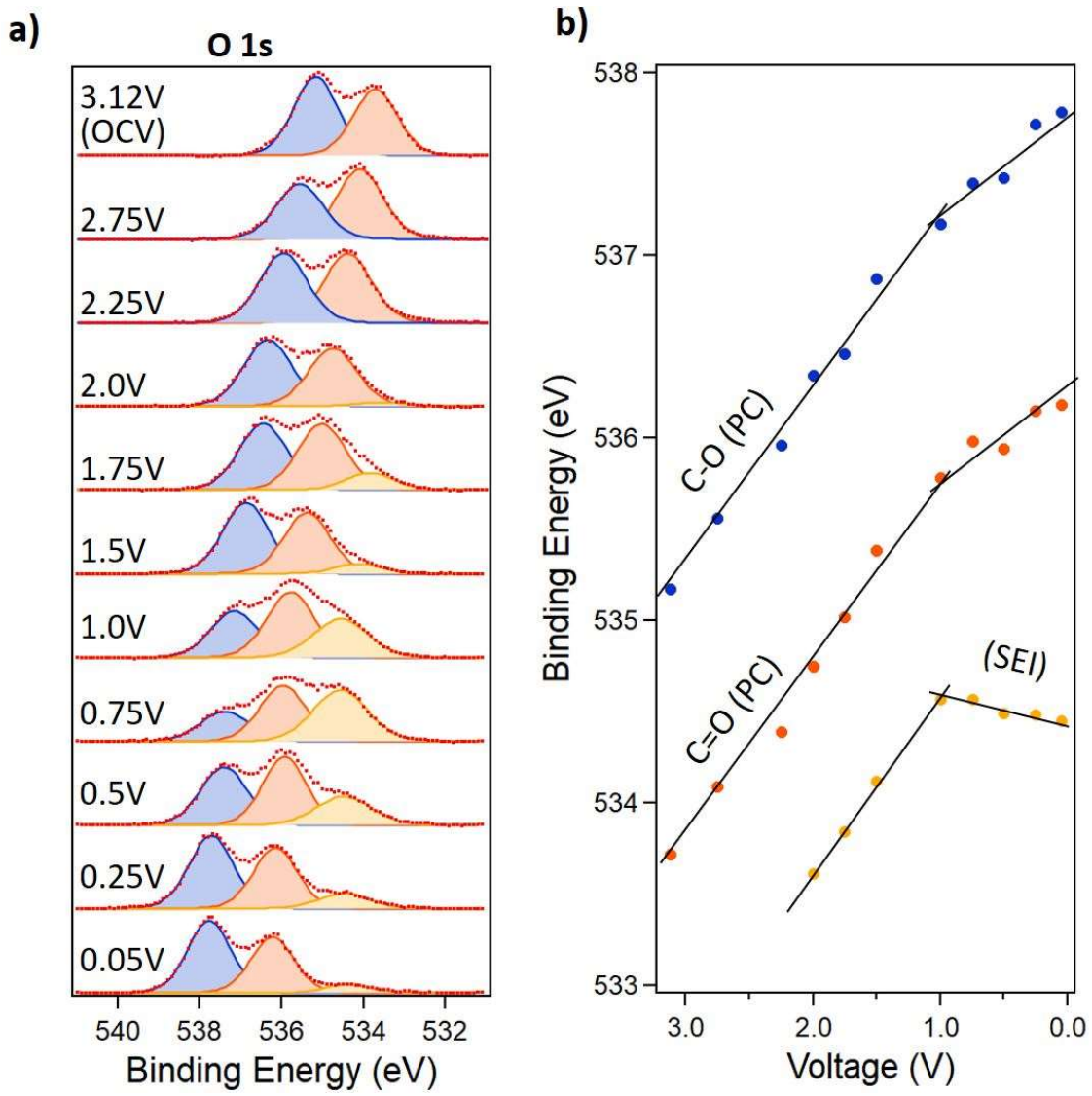

Figure 7 : **(a)** O 1s NAP-XPS spectra recorded on the thin electrolyte's precursor film as a function of the applied potential *vs.* Li^+/Li; **(b)** Evolution of the B.E. of O 1s components (without any B.E. calibration).

Moreover, considering the B.E. difference between this third O 1s component and the C 1s peak attributed to inorganic carbonates, this value ~241.8 eV remains almost constant during the whole experiment, which is the same difference as in Li_2CO_3 or in different lithium alkylcarbonates $ROCO_2Li$ [36]. Therefore, we can assign this O 1s component to inorganic carbonates, which validates our hypothesis.

Figure 8 displays F 1s spectra and the evolution of their B.E. as a function of the applied potential. At the beginning of the experiment (OCV and 2.75V) the F 1s spectra are composed

of a single peak attributed to $LiPF_6$. For potentials below 2.5V *vs.* Li^+/Li, an additional peak at lower B.E. assigned to LiF appears.

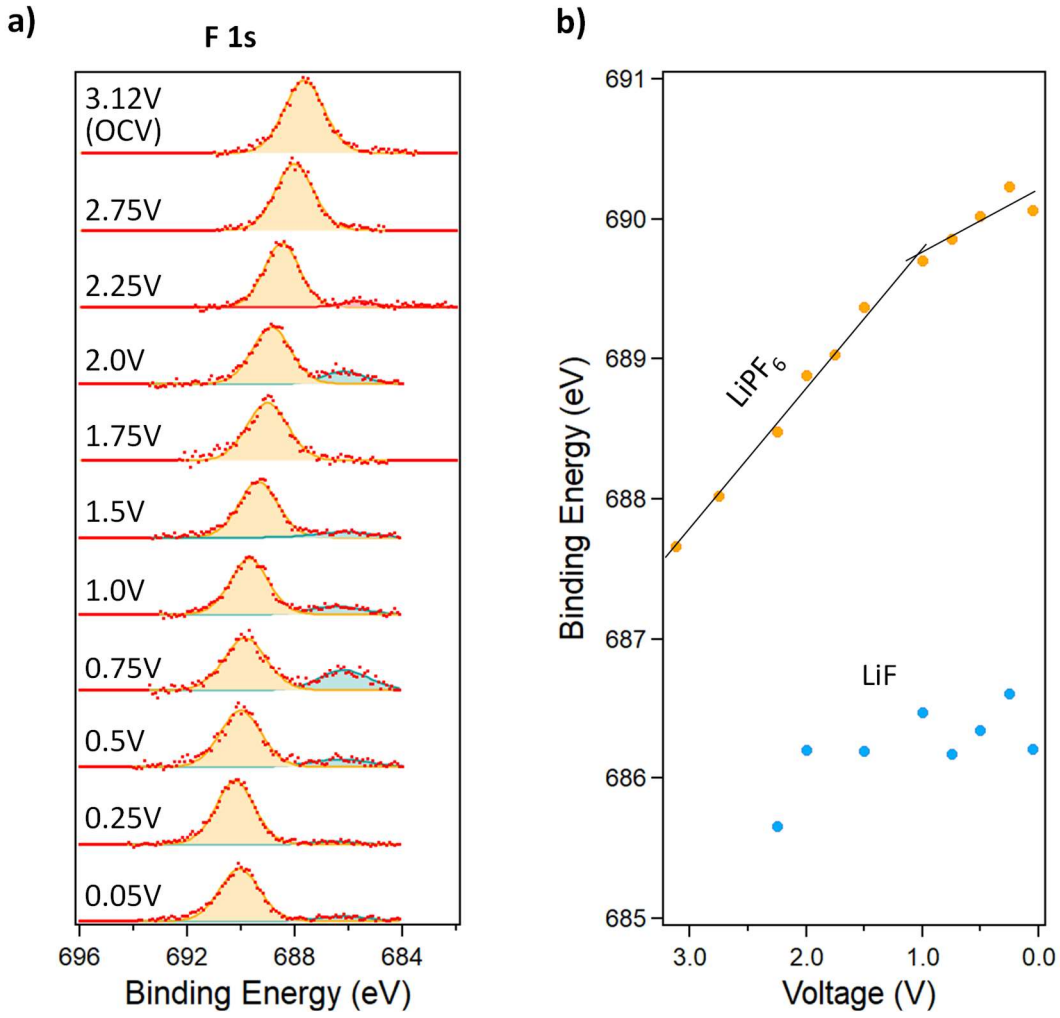

Figure 8 : **(a)** F 1s NAP-XPS spectra recorded on the thin electrolyte's precursor film as a function of the applied potential *vs.* Li^+/Li; **(b)** Evolution of the B.E. of F 1s components (without any B.E. calibration).

As shown in Figure 8b, the B.E. shift of $LiPF_6$ follows the same linear dependence as observed for other electrolyte species, *i.e.* + 1 eV/V for potentials greater than 1V and + 0.5 eV/V for potentials lower than 1V, whereas the B.E. of LiF is not affected by the applied potential (within the error due to its rather weak intensity and the poor signal-to-noise ratio). According to our model, this means that LiF is in direct electronic contact with the surface of the GC electrode, and therefore grounded with the spectrometer as well. Since LiF is an electronic insulator, this is possible only if its thickness is very low, otherwise the external parts

of the LiF layer would not be in electronic contact with the electrode. This is commonly observed for native oxide layers covering the surface of metals: when the oxide layer thickness is very low, its B.E. follows the same shift as the substrate if a potential is applied. Therefore, in our case LiF forms a very thin solid film at the surface of the GC electrode from the early stages of the electrochemical experiment and does not undergo the same spatial movement from the electrolyte to the electrode surface upon the formation of the SEI, like it is observed for other inorganic species. This is actually in good agreement with the behaviour we expect from this quite insoluble compound in the electrolyte.

This *operando* study was complemented by an *ex situ* XPS analysis of the GC electrode after the end of the dip & pull experiment (after the 0.05 V step). Once all NAP-XPS measurements were recorded, the analysis chamber was vented with dry argon, then the beaker containing the electrolyte was removed, and the analysis chamber was pumped to perform a classical *ex situ* XPS analysis in vacuum on the GC electrode surface. The obtained C 1s, O 1s and F 1s spectra are plotted in Fig. S4 and display very classical shapes (with no signature of the solvent), as commonly observed for SEI formation on a graphite electrode in a carbonate-based electrolyte.

Going back to the dip & pull experiment, a final observation in Figures 5 and 7 needs to be discussed. The linear shift observed for the inorganic carbonates in the higher voltage region (from OCV to 1V) is +1.1 eV/V, which is slightly higher than the expected 1 eV/V and observed for the electrolyte species (PC and $LiPF_6$ salt). It could be within the error of the measurement (± 0.1 eV/V), but another possible explanation is that the potential gradient in the EDL is modified by the presence of new species in the electrolyte, before the formation of the SEI. However, this hypothesis needs further investigation to be confirmed.

4. Conclusion

In this work, we have investigated the surface of a glassy carbon electrode and the surface of the electrolyte using an *operando* NAP-XPS approach. We were able to localize the thin electrolyte precursor film, which enables the simultaneous detection of the XPS signals from the glassy carbon electrode, the electrolyte and the SEI. The novelty of our work lies in the real-time observation of the SEI formation, enabled by *operando* XPS measurements, allowing for the identification of the main SEI species and giving an indirect access to their location in space (*i.e.* their distance to the electrode's surface) by following their binding energy shift as a

function of the applied potential. Our results confirm the formation of inorganic carbonates like Li_2CO_3, lithium alkylcarbonates and LiF, as reported in previous *ex situ* studies. To our knowledge, this is the first time the dynamic formation of the SEI is observed with access to chemical information. These results demonstrate that NAP-XPS is a powerful tool to investigate the SEI formation and stability in Li- and post-Li-ion batteries, paving the way for new studies on the effect of electrolyte additive and solvent mixture on the battery performances.

Acknowledgments

The authors acknowledge the French National Research Agency for its support through Labex STORE-EX project (ANR-10LABX-76-01). We acknowledge BATTERY 2030 and BIG-MAP projects funded by the European Union's Horizon 2020 research and innovation programme under Grant Agreements #957213 and 957189. We acknowledge MAX IV Laboratory for time on HIPPIE beamline under Proposal 20220354. We are grateful to Andrey Shavorskiy for his assistance during the experiments. Research conducted at MAX IV, a Swedish national user facility, is supported by the Swedish Research council under contract 2018-07152, the Swedish Governmental Agency for Innovation Systems under contract 2018-04969, and Formas under contract 2019-02496.

References

[1] E. Peled, *J. Electrochem. Soc.* 126 (1979) 2047
[2] R. Fong, U. Von Sacken, J. R. Dahn, *J. Electrochem. Soc.* 137 (1990) 2009
[3] J. O. Besenhard, H. Möhwald, J. J. Nickl, *Carbon* 18 (1980) 399
[4] Santner, H. J.; Korepp, C.; Winter, M.; Besenhard, J. O.; Moller, K. C., In-situ FTIR investigations on the reduction of vinylene electrolyte additives suitable for use in lithium-ion batteries. *Anal. Bioanal. Chem.* 379 (2004) 266-71
[5] Dopilka, A.; Gu, Y.; Larson, J. M.; Zorba, V.; Kostecki, R., Nano-FTIR Spectroscopy of the Solid Electrolyte Interphase Layer on a Thin-Film Silicon Li-Ion Anode. *ACS Appl Mater Interfaces* 15 (2023) 6755
[6] Källquist, I.; Le Ruyet, R.; Liu, H.; Mogensen,R.; Lee, M.-T.; Edström, K.; Naylor, A. J.; Advances in studying interfacial reactions in rechargeable batteries by photoelectron spectroscopy, *J. Mater. Chem. A*, 10 (2022) 19466
[7] Kalaga, K.; Shkrob, I. A.; Haasch, R. T.; Peebles, C.; Bareño, J.; Abraham, D. P., Auger Electrons as Probes for Composite Micro- and Nanostructured Materials: Application to Solid Electrolyte Interphases in Graphite and Silicon-Graphite Electrodes. *J. Phys. Chem. C* 121 (2017) 23333
[8] Lee, J. T.; Nitta, N.; Benson, J.; Magasinski, A.; Fuller, T. F.; Yushin, G., Comparative study of the solid electrolyte interphase on graphite in full Li-ion battery cells using X-ray photoelectron spectroscopy, secondary ion mass spectrometry, and electron microscopy. *Carbon* 52 (2013) 388
[9] Zhang, Z., et al. "Operando Electrochemical Atomic Force Microscopy of Solid-Electrolyte Interphase Formation on Graphite Anodes: The Evolution of SEI Morphology and Mechanical Properties." *ACS Appl Mater. Interfaces* 12 (2020) 35132
[10] Wang, L.; Deng, X.; Dai, P. X.; Guo, Y. G.; Wang, D.; Wan, L. J., Initial solid electrolyte interphase formation process of graphite anode in $LiPF_6$ electrolyte: an in situ ECSTM investigation. *Phys Chem Chem Phys* 14 (2012) 7330-6
[11] Kitz, P. G.; Lacey, M. J.; Novak, P.; Berg, E. J., Operando EQCM-D with Simultaneous in Situ EIS: New Insights into Interphase Formation in Li Ion Batteries. Anal. Chem. 91 (2019) 2296
[12] P. Novák, F. Joho, R. Imhof, J.-C. Panitz, O. Haas, *J. Power Sources*, 81-82 (1999) 212
[13] S. H. Ng, C. Vix-Guterl, P. Bernardo, N. Tran, J. Ufheil, H. Buqa, J. Dentzer, R. Gadiou, M. E. Spahr, D. Goers, P. Novák, *Carbon* 47 (2009) 705
[14] Z. Zhang, D. Fouchard, J. R. Rea, *J. Power Sources* 70 (1998) 16
[15] Leskes, M.; Kim, G.; Liu, T.; Michan, A. L.; Aussenac, F.; Dorffer, P.; Paul, S.; Grey, C. P., Surface-Sensitive NMR Detection of the Solid Electrolyte Interphase Layer on Reduced Graphene Oxide. J. Phys. Chem. Lett. 8 (2017) 1078
[16] Castaing, R.; Moreau, P.; Reynier, Y.; Schleich, D.; Jouanneau Si Larbi, S.; Guyomard, D.; Dupré, N., NMR quantitative analysis of solid electrolyte interphase on aged Li-ion battery electrodes. *Electrochimica Acta* 155 (2015) 391
[17] G. Ketteler, D.F. Ogletree, H. Bluhm, H.J. Liu, E.L.D. Hebenstreit, M. Salmeron, *J. Am. Chem. Soc.* 127 (2005) 18269
[18] G. Ketteler, S. Yamamoto, H. Bluhm, K. Andersson, D.E. Starr, D.F. Ogletree, H. Ogasawara, A. Nilsson, M. Salmeron, *J. Phys. Chem. C* 111 (2007) 8278
[19] H. Siegbahn, Electron Spectroscopy for Chemical Analysis of Liquids and Solutions. *J. Phys. Chem. B*, 89 (1985) 897
[20] A. Naitabdi et al., CO oxidation activity of pt, zn and ZnPt nanocatalysts: A comparative study by: In situ near-ambient pressure X-ray photoelectron spectroscopy. Nanoscale, 10 (2018) 6566
[21] S. Axnanda et al., Using "Tender" X-ray ambient pressure X-ray photoelectron spectroscopy as a direct probe of solid-liquid interface. Sci. Rep. 5 (2015) 9788.
[22] J. Maibach, I. Källquist, M. Andersson, S. Urpelainen, K. Edström, H. Rensmo, H. Siegbahn, M. Hahlin, Probing a Battery Electrolyte Drop with Ambient Pressure Photoelectron Spectroscopy, *Nat. Commun.* 2019, 10, 10803.
[23] P. M. Dietrich, L. Gehrlein, J. Maibach, A. Thissen, Probing Lithium-Ion Battery Electrolytes with Laboratory Near-Ambient Pressure XPS, Crystals 10 (2020) 1056
[24] Källquist, I.; Lindgren, F.; Lee, M.-T.; Shavorskiy, A.; Edström, K.; Rensmo, H.; Nyholm, L.; Maibach, J.; Hahlin, M. Probing Electrochemical Potential Differences over the Solid/Liquid Interface in Li-Ion Battery Model Systems. *ACS Appl. Mater. Interfaces* 13 (2021) 32989
[25] I. Källquist, T. Ericson, F. Lindgren, H. Chen, A. Shavorskiy, J. Maibach, M. Hahlin, Potentials in Li-Ion Batteries Probed by Operando Ambient Pressure Photoelectron Spectroscopy, ACS Appl. Mater. Interfaces 14 (2022) 6465
[26] de Gennes, P. G.; Wetting: statics and dynamics, *Rev. Mod. Phys.* 57 (1985) 827
[27] Cazabat, A., Gerdes, S., Valignat, M. *et al.* Dynamics of Wetting: From Theory to Experiment. *Interface Science*, 5 (1997) 129
[28] Bonn, D., Eggers, J., Indekeu, J., Meunier, J., Wetting and spreading, *Reviews of Modern Physics*, 81 (2009) 739
[29] P. Novák, F. Joho, R. Imhof, J.-C. Panitz, O. Haas, In situ investigation of the interaction between graphite and electrolyte solutions, *J. Power Sources* 81-82 (1999) 212
[30] S. Pérez-Villar, P. Lanz, H. Schneider, P. Novák, Characterization of a model solid electrolyte interphase/carbon interface by combined in situ Raman/Fourier transform infrared microscopy, *Electrochimica Acta* 106 (2013) 506
[31] G. Zampardi, F. La Mantia, W. Schuhmann, Determination of the formation and range of stability of the SEI on glassy carbon by local electrochemistry, *RSC Adv.*, 5 (2015) 31166
[32] Zhu, S. et al. Hippie: A New Platform for Ambient-Pressure X-Ray Photoelectron Spectroscopy at the Max IV Laboratory. *J. Synchrotron Radiat.* 28 (2021) 624
[33] Bard, A. J.; Faulkner, L. R.; "Electrochemical Methods - Fundamentals and Applications", John Wiley and Sons, New York, 1980, Chapter 12, Double-Layer Structure and Adsorbed Intermediates in Electrode Processes, p. 488-515
[34] Yan, C.; Li, H.-R.; Chen, X.; Zhang, X.-Q.; Cheng, X.-B.; Xu, R.; Huang, J.-Q.; Zhang, Q.; Regulating Inner Helmholtz Plane for Stable Solid Electrolyte Inter-phase on Lithium Metal Anodes, *J. Am. Chem. Soc.* 141 (2019) 9422

[35] Yan, C.; Xu, R.; Xiao, Y.; Ding, J.-F.; Xu, L.; Li, B.-Q.; Huang, J.-Q.; Toward Critical Electrode/Electrolyte Interfaces in Rechargeable Batteries, *Adv. Funct. Mater.* 30 (2020) 1909887

[36] Dedryvère, R.; Gireaud, L.; Grugeon, S.; Laruelle, S.; Tarascon, J.-M.; Gonbeau, D.; Characterization of lithium alkyl carbonates $ROCO_2Li$ by X-ray photoelectron spectroscopy (XPS) : experimental and theoretical study, *J. Phys. Chem. B*, 109 (2005) 15868

Supplementary information

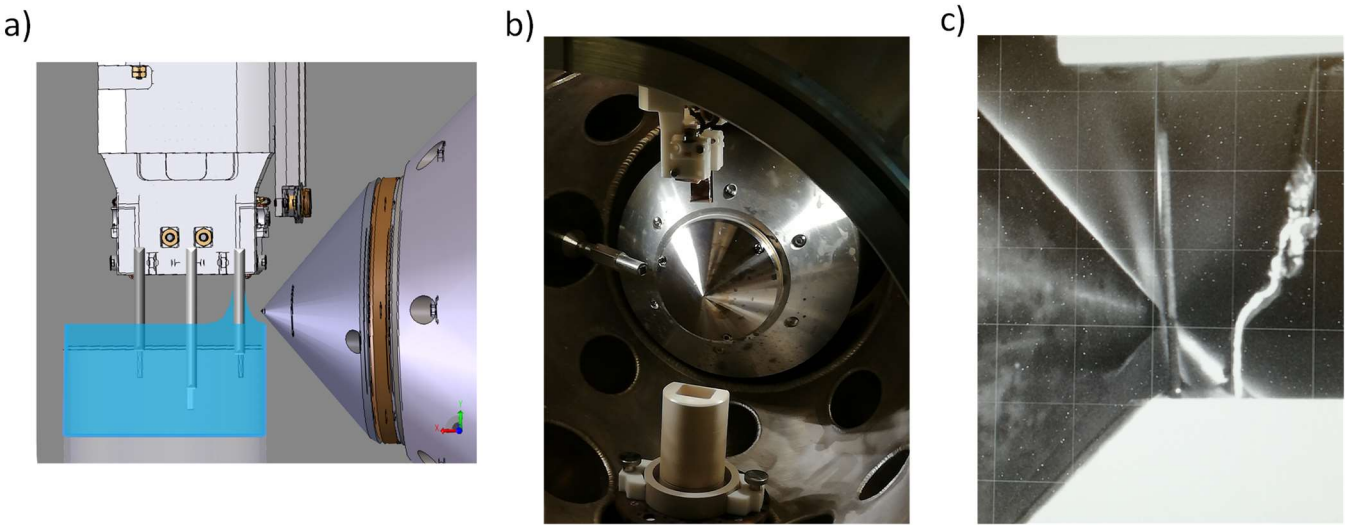

Figure S1 : Experimental dip and pull setup: (a) and (b) Schematic view and photo of the electrochemical cell and photoelectron analyzer; (c) Photo taken during the experiment.

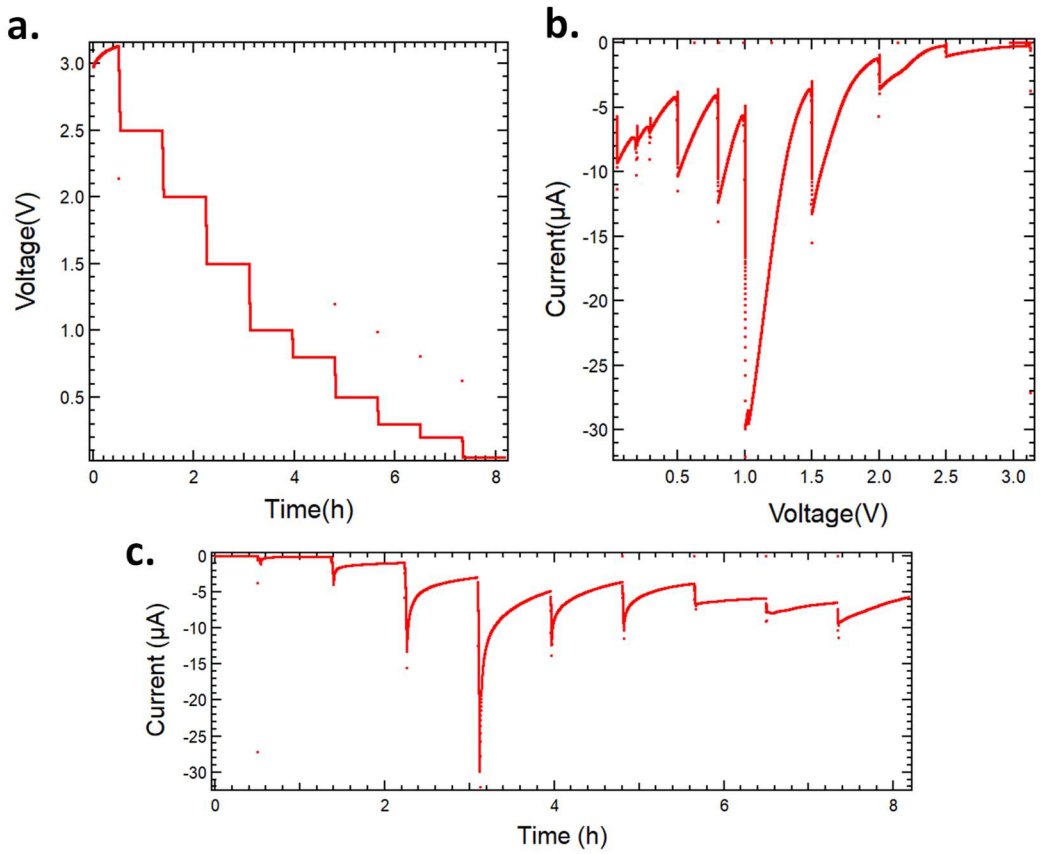

Figure S2 : Electrochemical behaviour of the cell in the in-house argon glovebox: **(a)** Voltage *vs.* time profile applied from OCV (Open Circuit Voltage) to 0.05 *vs.* Li^+/Li; **(b)** Resulting current intensity *vs.* voltage curve; **(d)** Variation of the current intensity *vs.* time.

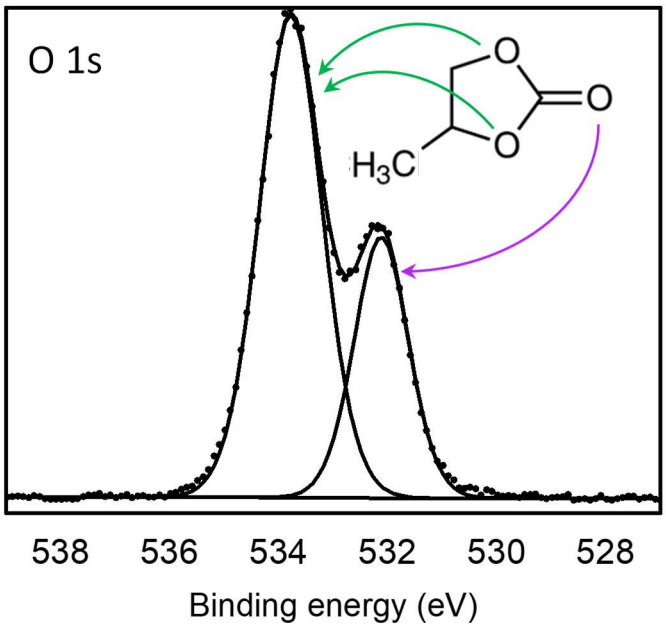

Figure S3 : O 1s spectrum of pure PC solvent, as a frozen liquid drop at T = -140°C under ultra-high vacuum (in-house XPS spectrometer at hν = 1486.7 eV).

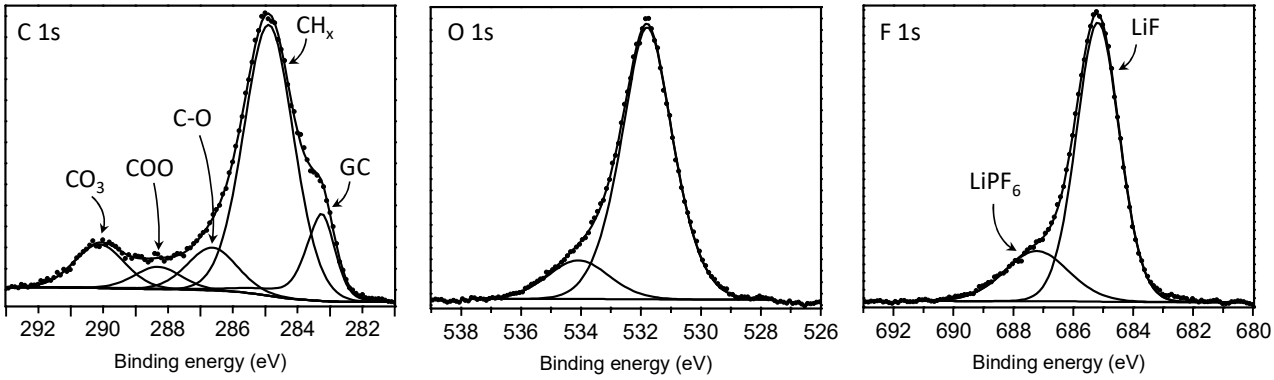

Figure S4 : *Ex situ* XPS C 1s, O 1s and F 1s spectra of the GC electrode's surface, recorded in vacuum after the end of the *operando* dip & pull experiment (which was stopped at 0.05 V applied potential).